Interaction of the Solar Wind with Unmagnetized Planets

Zoltan Dobe,[1] Kevin B. Quest,[2] Vitali D. Shapiro,[2,3] Karoly Szego,[1] and Joseph D. Huba[4]

[1]*KFKI Research Institute for Particle and Nuclear Physics, Budapest, Hungary*

[2]*ECE Department, University of California San Diego, La Jolla, California 92093*

[3]*Department of Physics, University of California San Diego, La Jolla, California 92093*

[4]*Plasma Physics Division, Naval Research Laboratory, Washington, D.C. 20375*

The results of a one-dimensional electromagnetic hybrid simulation of the interaction between the ionospheres of Venus and Mars and the solar wind are presented. Finite electron inertia is retained, allowing for the analysis of the lower hybrid waves propagating along an oblique but fixed angle to the shocked solar-wind magnetic field. The waves are excited by a relative drift between a cold electron beam, created by $\mathbf{E} \times \mathbf{B}$ pickup, and the planetary oxygen ions. The free energy source for instability is in the solar-wind proton flow supporting electron drift through the convective electric field. The waves generate a collective friction between the shocked solar-wind flow and planetary ions.

Because Venus and Mars do not possess a significant intrinsic magnetic field, the ionosphere is the main, however weak, obstacle to the solar-wind flow, and the planetary bow shocks are located quite close to the planets. The ionospheres of both planets are directly exposed to the streaming shocked solar wind. Data from the particle and wave instruments onboard the Pioneer Venus Orbiter (PVO) and Phobos-2 spacecraft show the existence of a thin $\Delta \sim 100$ km turbulent transition region between the shocked solar wind and the ionospheres of Venus and Mars, referred to as the plasma mantle [1]. In the mantle, plasmas of both solar wind and ionospheric origin are present in comparable densities $n = 10^2$ cm^{-3}, but with very different temperatures. The solar-wind proton (electron) temperature is approximately 100 (30) eV, and the drift velocity is close to the proton thermal velocity. The planetary oxygen and electron temperature is close to 1 eV. There is also experimental evidence for the presence of superthermal oxygen [2] and electron populations [3,4] at Mars and Venus. Large tailward escape of planetary ions, most probably originating from the dayside mantle, was also observed at Mars [5].

Since the mantle thickness is much less than the ion gyroradius, the usual scheme of $\mathbf{E} \times \mathbf{B}$ pickup of the planetary ions by the solar wind is not applicable. The scenario that collective friction due to waves must be responsible for the observed tailward ion escape was formulated first for the Mars mantle in [6], and then for the Venus mantle [7]. This point of view is now widely accepted in other papers [8–10]. Intense wave activity was observed at the dayside Venusian mantle by the 100 Hz channel of the electric field detector on the PVO, with typical average amplitudes around tens of mV/m [11]. Even stronger wave activity in the 5−50 Hz frequency range was measured at the boundary of the Mars ionosphere [12].

The modified two stream instability (MTSI) [6–8] and the ion acoustic current driven instability [13] have both been suggested as explanations of the observed wave activ-

ity. The scenarios of wave activity developing from these two instabilities are quite different. The MTSI results in the excitation of sufficiently long wavelength oscillations with the typical wavelength of the order of the solar-wind electron gyroradius and frequencies in the vicinity of the lower hybrid frequency ω_{LH}. This frequency is equal to a geometrical mean of the electron and proton gyrofrequencies (30–40 Hz for mantle conditions). At the same time, waves excited by ion acoustic instability are with much shorter wavelengths, of the order of electron Debye length, and with higher frequencies of the order of an ion plasma frequency (~ 1 kHz for mantle conditions). An ion acoustic scenario has been supported by the interpretation of PVO wave data proposed in Ref. [14]. Authors of this reference analyzed peak values of wave data in PVO crossings of ionopause. The signal was always strongest in the 100 Hz channel; however, it was pointed out that background noises due to the variation of plasma environment, especially rapid variations of the Debye length at the ionopause, may be generated, contributing to 100 Hz signals. This led to the conclusion that the main part of wave emission may be of the ion acoustic-type at frequencies $\lesssim 1$ kHz. At the same time the averaging procedure used in [8] for wave data from approximately 50 orbits demonstrated that the 100 Hz signal is dominant and real. Finally, a full statistical analysis of the peak values of the wave data performed recently in [9] are well correlated with ionopause crossings. While the above mentioned change in background noise level near the ionopause is still considered as important, it is generally agreed now that the peak at 100 Hz is not excluded from being natural. Therefore experimental data demonstrate a necessity of a theoretical model responsible for the 100 Hz signal.

It is noteworthy to mention the existence of another problem with the existence of ion acoustic instability in the real mantle. The model was originally developed for a three component plasma (protons, ions, and solar-wind electrons), and the presence of cold planetary electrons has

    0031-9007/99/83(2)/260(4)$15.00   © 1999 The American Physical Society

a strong stabilizing effect on ion acoustic instability. It has been shown that even a relative abundance of 10^{-1} cold electrons can stabilize this oscillation branch [15].

Analysis of the dispersion relation of the MTSI including two ion and two electron species (corresponding to the solar wind and ionospheric components) has been performed in [8]. It was concluded that two types of MTSI branches are unstable. In the vicinity of the lower hybrid frequency, there is a fluid-type branch corresponding to waves propagating perpendicular to the magnetic field. At the same time, more high frequency wave data may be attributed to a kinetic branch of the MTSI, corresponding to the waves propagating obliquely to the magnetic field, and having frequencies several times above the lower hybrid frequency.

In the present Letter we propose a new, faster developing type of MTSI that better matches PVO data. For this branch of MTSI, waves are generated by the interaction between the ionospheric oxygen ions and the cold electron beam, created by $\mathbf{E} \times \mathbf{B}$ pickup. Electron pickup takes place over a few electron gyroperiods, a time interval much shorter than the lower hybrid period. Although the cold electron beam has a little kintetic energy of its own, the wave particle resonance is sustained for a longer time due to electron pickup under the combined action of the magnetic and convective electric field of the solar wind. This makes possible a substantial transfer of free energy from the proton flow to the waves.

The excited waves are predominantly electrostatic $\omega_{pe} < kc$, where ω_{pe} is the electron plasma frequency, and k is the wave number. They propagate in a wide range of angles $\theta \sim 60°$–$90°$ to the external magnetic field, and, contrary to the model proposed in [8], they couple planetary ions with solar-wind flow already at the initial linear stage of MTSI.

A dispersion relation describing wave excitation can be written as follows:

$$\frac{\omega_{pe}^2}{\omega_{ce}^2}\left(1 + \frac{\omega_{pe}^2}{k^2 c^2}\right) - \frac{\omega_{pe}^2}{(\omega - ku_e)^2}\frac{k_{\parallel}^2 c^2}{k^2 c^2 + \omega_{pe}^2} +$$
$$\frac{1 + w_p Z(w_p)}{k^2 D_p^2} + \frac{1 + w_i Z(w_i)}{k^2 D_i^2} = 0 . \tag{1}$$

A similar dispersion relation for two component plasma (a proton flow through electrons) has been derived in [16] in hydrodynamical approximation; kinetic effects were taken into account in [8]. In Eq. (1) we made the same assumptions as in the numerical simulation about the presence of only one component of cold fluid electrons. Both protons and heavy ions are treated kinetically. The following notations are used:

$$w_p = \frac{\omega - ku_p}{k\nu_{Tp}}, \qquad w_i = \frac{\omega}{k\nu_{Ti}},$$

and

$$Z(z) = \int_{-\infty}^{\infty} d\zeta\, \frac{\exp(-\zeta^2)}{\zeta - z}$$

is the dispersion function. The notation $\nu_{Tp}(\nu_{Ti})$ is the thermal velocity for protons (ions), and u_e, u_p the drift velocities of electrons and protons are used. Wave frequency satisfies the condition $\omega_{cp} < \omega < \omega_{ce}$, where ω_{cp}, ω_{ce} are the proton and electron gyrofrequencies. Correspondingly, electrons are magnetized in these oscillations, while protons and ions are not.

The most unstable mode corresponds to the case when Doppler shifted wave frequency $(\omega - ku)$ coincides with the frequency of the plasma eigenmode, in our case, of the whistler mode. An instability is similar to the well-known Buneman instability [17] in unmagnetized plasma, when Doppler shifted wave frequency coincides with Langmuir frequency. The same way as for the Buneman instability $|\omega| \ll ku$, and the resonance condition can be written as

$$ku_e = \omega_{ce} \frac{k_{\parallel} kc^2}{k^2 c^2 + \omega_{pe}^2} . \tag{2}$$

A numerical solution of the dispersion relation is presented in Fig. 1. The growth rate of the most unstable mode, satisfying condition (1), is plotted as a function of the mode frequency. A parameter which changes along this curve is $\kappa = (k_{\parallel}/k)\sqrt{m_p/m_e}$, i.e., an angle at which the wave is propagating in respect to the ambient magnetic field. For $\kappa > 1$ frequency grows almost linearly with κ, while the growth rate reaches its maximum at $\kappa = 6$ and then slowly decreases. Triangles in the figure show the values of frequency and growth rate of the most unstable mode obtained in the numerical simulation for the different values of κ listed in the figure. As can be seen, analytical and simulation results are in good agreement.

We have investigated the linear and nonlinear evolution of the above described MTSI branch, using the hybrid particle simulation method. The simulation results are obtained with a one-dimensional hybrid kinetic code described in Ref. [18]. The code treats the two ion species (protons and oxygen) using particle-in-cell methods while the electrons are modeled as a fluid in which inertial and electromagnetic effects are retained. It conserves total energy and momentum with an accuracy better than 1%. The
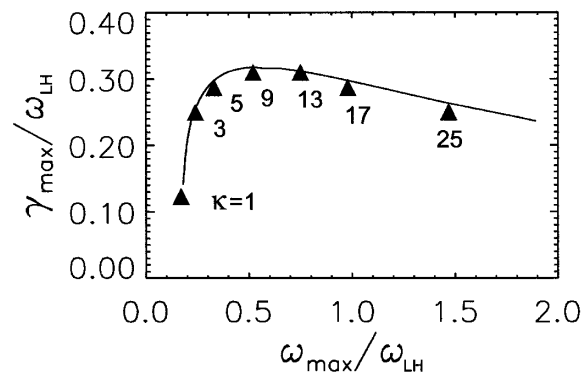
FIG. 1. Relationship between the maximum growth rate and corresponding real frequency for different κ values. Solid line is calculated from the dispersion equation (2), triangles correspond to simulation results.

frame, boundary conditions (periodic in x), and initialization (uniform relative drift between Maxwellian protons and ions) of the simulation are the same as that used in Ref. [18], with the difference that waves are allowed to propagate at an arbitrary angle with respect to the ambient magnetic field. The parameters used in the simulation are following. The solar-wind flow is initialized with an x-directed drift velocity $u_p = 1.2\nu_{Tp'}$, where $\nu_{Tp} = \sqrt{T_p/m_p}$. The density of the protons and the planetary ions are chosen to be the same, and β values for the different plasma components are $\beta_p = 0.8$, $\beta_i = 0.0032$, and $\beta_e = 0.016$, where β_j is the ratio of the thermal pressure to the magnetic field pressure for the jth species. If we assume the electron number density n_e of 10^2 cm^{-3}, then simulations correspond to the case of $T_p = 100$ eV, $T_e = 1$ eV, $T_i = 0.2$ eV, $u_p = 120$ km/s, and $B \approx 50$ nT. Conditions of quasineutrality $n_e = n_p + n_i$ and the zero net current in the flow (x) direction $u_e = n_p u_p/n = (1/2)u_p$ are imposed into the simulations. The latter condition is a consequence of one dimensionality and the assumption about the absence of the magnetic field shear. Releasing a condition of zero net current in the analytic dispersion relation, it is possible to prove that this condition does not alter the evolution of instability, at least at its linear stage.

Results of simulations are shown in Figs. 2 and 3. In this paper we concentrate on the cases such that $\kappa > 1$. Smaller κ values yield results similar to those obtained in [18], and will not be discussed here.

Figure 2 illustrates an evolution in time of the bulk momentum of the solar-wind protons [Fig. 2(a)], and the bulk momentum of the planetary oxygen ions [Fig. 2(b)]. Both are normalized to the total initial bulk momentum of protons in the x direction. In Fig. 2(c) the linear and nonlinear evolution of the total wave energy density normalized to the total initial kinetic energy is shown. Wave energy was approximated by the formula,

$$W_{\text{wave}} = \sum_k \omega_k \frac{\partial D}{\partial \omega_k} \frac{|E_k|^2}{8\pi} \approx \frac{\omega}{ku_e} \frac{\omega_{pe}^2}{\omega_{ce}^2} \frac{E_x^2}{4\pi}. \quad (3)$$

The dispersion relation (1) can be written as $D = 0$, and the large factor $\omega_{pe}^2/\omega_{ce}^2 = 3 \times 10^3$ appears in (3) due to the input of the kinetic energy of the transverse electron oscillations.

In Fig. 2 each line style corresponds to different κ values: $\kappa = 1$, solid line; $\kappa = 3$, dotted line; and $\kappa = 17$, dot-dashed line. Note that significant momentum exchange between the two ion species is induced by waves for a wide range of propagation angles. These results also demonstrate that the efficiency of momentum coupling between solar wind and ionospheric plasma decreases as the angle between the magnetic field and solar-wind flow increases. This is similar to the behavior of the saturation level of wave energy. The saturated wave energy varies in the range of a few percent up to $\sim 25\%$ of the initial kinetic energy. The average amplitude of the saturated electric field oscillations, $\sqrt{\langle E_x^2 \rangle}$ can be estimated as 10–50 mV/m.
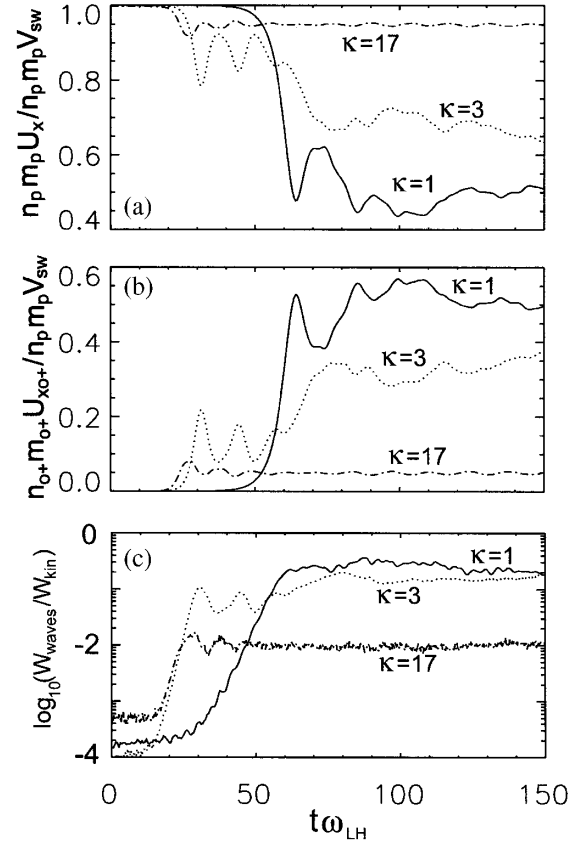
FIG. 2. Evolution in time of the bulk momentum for solar-wind protons (a), of oxygen ions (b) (both normalized to initial proton bulk momentum), and of the wave energy (c) normalized to the initial total kinetic energy of protons for different κ values: $\kappa = 1$, solid line; $\kappa = 3$, dotted line; $\kappa = 17$, dot-dashed line.

As it follows from the resonance condition (2) with the deceleration of the electron beam, the instability shifts to a larger k resulting in a significant broadening of the wave spectrum to a higher ω, a feature observed in simulations at the nonlinear stage of instability.

Figure 3 displays the phase space plots (left column) and corresponding velocity distributions (right column) for both protons and oxygen ions for the case of $\kappa = 3$. The times chosen correspond to the beginning of the nonlinear phase $t\omega_{\text{LH}} = 30$ for Fig. 3(a) and to the turbulent phase $t\omega_{\text{LH}} = 150$ for Fig. 3(b). Velocities in the x direction are normalized to the proton thermal velocity, and distances to $\rho^* = (1/\omega_{ce})\sqrt{T_p/m_e}$.

The presence of well-developed vortices in the phase space of protons suggests that saturation of the instability takes place via electrostatic trapping. Nevertheless, only the low velocity part of the proton beam is trapped, and the saturation mechanism can be described as follows. The electron drift which is a driver for the instability is supported by a convective electric field $\mathbf{E}_c$ produced by the solar-wind flow across magnetic field lines $\mathbf{E}_c = -(1/c)(\mathbf{u} \times \mathbf{B})$. When $(\Delta u_e/u_e) \sim (\Delta E_c/E_c) \sim \sqrt{e\varphi/m_p u_e^2} \sim \gamma/ku_e$, the linearly unstable
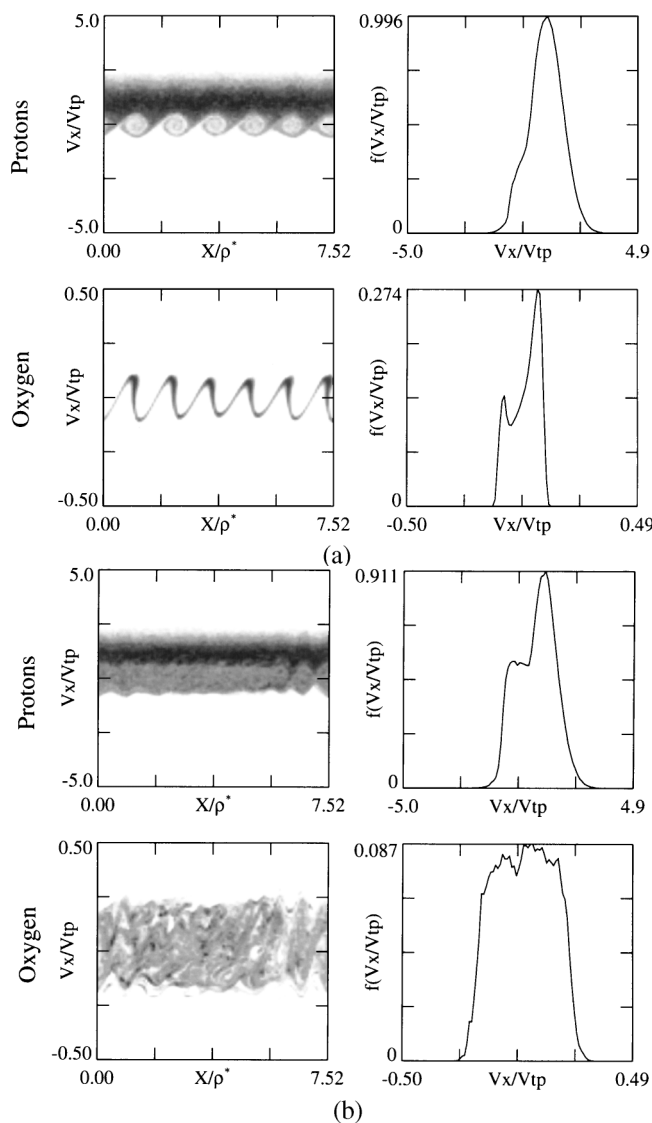
FIG. 3. Phase space (left column) and velocity distribution (right column) of the protons and oxygen ions at (a) the saturation of the linear growth phase, and (b) the well-developed turbulent phase.

monochromatic wave loses resonance with the beam and saturates. In our model an electron beam is strongly coupled with the proton flow, and a beam deceleration is determined by the proton inertia. The condition for saturation corresponds to the wave energy

$$W = \frac{\omega}{ku_e} \frac{\omega_{pe}^2}{\omega_{ce}^2} \frac{k^2\varphi^2}{4\pi} \approx \frac{\gamma^4\omega}{\omega_{LH}^5} \kappa^{-3} n_0 m_p u_e^2, \quad (4)$$

which is close to the simulation results and also decreases with the growth of κ. Note that due to their larger mass, oxygen ions are trapped more slowly by the waves than protons, and this is why vortices cannot be observed in the oxygen phase space density plot at the presented stage. At later times nonlinear wave effects overlap the vortices, resulting in a transfer of beam-directed energy into thermal

motion. Heating of the two ion species is also shown. It results in the broadening of their velocity distribution functions. This is especially pronounced in the case of the heavy ion population, where the energetic tail can reach velocities comparable to the proton thermal velocity. This is consistent with PVO's superthermal oxygen ion measurements [2] and the large number of planetary pickup ions detected by Phobos-2. This is well within the distance needed for an $\mathbf{E} \times \mathbf{B}$ energization [5].

We can draw the conclusion that the presented fluidlike branch of MTSI driven by the $\mathbf{E} \times \mathbf{B}$ pickup of planetary electrons can strongly couple the solar wind to the ionospheric plasma in both energy and momentum. There are several improvements of the model to be made in the future in order to further match this mechanism to observations. We need to use simulation models with nonperiodic boundary conditions so that a constant injection of the solar-wind protons in the simulation box can take place, and the instability will be saturated in distance, not in time. Inclusion of electron particle effects, such as Landau damping, should also be studied. This will necessitate the use of the particle simulation codes for electrons. Finally, the model should be extended to multiple spatial dimensions with nonperiodic boundary conditions to be able to examine the effect of the finite height of the mantle region as well as the wave spectral modifications introduced by the observed shear in the magnetic field.

[1] K. Spenner et al., J. Geophys. Res. **7**, 655 (1980).
[2] H. A. Taylor et al., J. Geophys. Res. **7**, 765 (1980).
[3] N. M. Shutte et al., Nature (London) **341**, 614 (1989).
[4] K. Szego et al., J. Geophys. Res. **102**, 2175 (1997).
[5] H. Rosenbauer et al., Nature (London) **341**, 612 (1989).
[6] R. Z. Sagdeev et al., Geophys. Res. Lett. **17**, 663 (1990).
[7] K. Szego et al., Geophys. Res. Lett. **18**, 305 (1991).
[8] V. D. Shapiro et al., J. Geophys. Res. **100**, 21 289 (1995).
[9] R. J. Strangeway and C. T. Russell, J. Geophys. Res. **101**, 17 313 (1996).
[10] H. Perez de Tejada J. Geophys. Res. **103**, 31 499 (1998).
[11] F. L. Scarf et al., J. Geophys. Res. **85**, 7599 (1980).
[12] R. Grard et al., Nature (London) **341**, 607 (1989).
[13] J. D. Huba, Geophys. Res. Lett. **20**, 1751 (1993).
[14] Crawford et al., in *Plasma Environment of Non-Magnetic Planets,* edited by T. I. Gombosi (Pergamon Press, Oxford, 1993), p. 253.
[15] K. Szego et al. (to be published).
[16] J. B. McBride et al., Phys. Fluids **15**, 2367 (1972).
[17] O. Buneman, Phys. Rev. **115**, 503 (1959).
[18] K. B. Quest et al., Geophys. Res. Lett. **24**, 301 (1997).